DRAFT VERSION NOVEMBER 6, 2006
Preprint typeset using LaTeX style emulateapj v. 10/09/06

LARGE MAGNETIC FIELDS AND MOTIONS OF OH MASERS IN W75 N

VINCENT L. FISH[1] & MARK J. REID[2]

Draft version November 6, 2006

ABSTRACT

We report on a second epoch of VLBA observations of the 1665 and 1667 MHz OH masers in the massive star-forming region W75 N. We find evidence to confirm the existence of very strong ($\sim$ 40 mG) magnetic fields near source VLA 2. The masers near VLA 2 are dynamically distinct and include a very bright spot apparently moving at 50 km s^{-1} relative to those around VLA 1. This fast-moving spot may be an example of a rare class of OH masers seen in outflows in star-forming regions. Due to the variability of these masers and the rapidity of their motions, tracking these motions will require multiple observations over a significantly shorter time baseline than obtained here. Proper motions of the masers near VLA 1 are more suggestive of streaming along magnetized shocks rather than Keplerian rotation in a disk. The motions of the easternmost cluster of masers in W75 N (B) may be tracing slow expansion around an unseen exciting source.

Subject headings: masers — ISM: kinematics and dynamics — stars: formation — magnetic fields — ISM: individual (W75 N) — radio lines: ISM

1. INTRODUCTION

W75 N is a complex massive star-forming region with many sites of star formation and masers (e.g., Persi et al. 2006). W75 N (B) is composed of at least four continuum sources, of which VLA 1 and VLA 2 host both OH and H_2O masers (Hunter et al. 1994; Torrelles et al. 1997). The H_2O masers around VLA 2 appear to be located on a shell with an expansion velocity of $\sim$ 28 km s^{-1} (Torrelles et al. 2003) and organized substructure on scales as small as 1 AU (Uscanga et al. 2005). The sources VLA 1, VLA 2, and VLA 3 are all believed to drive large-scale molecular outflows (Shepherd et al. 2003, 2004, and references therein).

The OH masers in W75 N were first observed interferometrically by Harvey et al. (1974), who noted three different sites of OH maser emission. VLBI techniques were first employed in this source by Haschick et al. (1981). The full large-scale distribution of masers, including the easternmost cluster and the group near VLA 2, was detected by Baart et al. (1986). Extreme variability of OH maser features in W75 N was noted by Alakoz et al. (2005), who reported that a flare up to 750 Jy was briefly the brightest OH maser in the sky. Flaring is also seen in many of the water (Lekht & Krasnov 2000, and references therein) and methanol masers in this source (Goedhart et al. 2004). The OH masers near VLA 2 appear to have a much larger velocity scatter than do the rest of the masers in W75 N (B) (Fish et al. 2005). It is in the aim of exploring the kinematic differences between the masers in VLA 1 and VLA 2 that we revisit the region with VLBA observations.

2. OBSERVATIONS

The VLBA was used to observe the 1665.4018 and 1667.3590 MHz transitions of OH in W75 N (G81.871+0.781) on 2000 November 22 and 2001 January 06 (data combined; hereafter, epoch 1). For each frequency, dual-circular polarization observations were taken using a 125 kHz bandwidth divided into 128 spectral channels (corresponding to a velocity width of 0.176 km s^{-1}), centered on v_{LSR} = 10 km s^{-1} (radio). Further details of these observations as well as the resulting images can be found in Fish et al. (2005). A second epoch of data was taken on 2004 September 16 and 19. Observational parameters were identical, with the exception that the bandwidth was centered at v_{LSR} = 7 km s^{-1}. The synthesized beam size was approximately 9.0×6.5 mas with a blank sky rms noise of 8 mJy beam^{-1}. In this work we report both on the second epoch of observations and observed changes in W75 N between the two epochs.

3. RESULTS

We recover a total of 123 maser features (lines), approximately the same as the 120 features detected in epoch 1 in the same amount of on-source observing time (Fish et al. 2005). Spot parameters are listed in Table 1. A map of detected maser emission is shown in Figure 1. Our velocity coverage includes most of the brightest features but is not sufficient to have seen all known maser features in this source, which range from –4.9 km s^{-1} (Hutawarakorn et al. 2002) up to +33 km s^{-1} (Yngvesson et al. 1975). The map is qualitatively similar to epoch 1 (Fig. 27 of Fish et al. 2005) except near VLA 2 (Fig. 2 of the present work).

The magnetic fields we infer from Zeeman splitting of left- and right-circular polarization (LCP and RCP) components are shown in Figure 1 and listed in Table 2. The strength and line-of-sight direction of the magnetic fields are consistent with values obtained in the epoch 1, except near source VLA 2. Our velocity coverage is too small to detect both Zeeman components at 1665 MHz (and at 1667 MHz, depending on the systemic velocity) when split by $\sim$ 40 mG, as seen by Slysh & Migenes (2006) near VLA 2. However, we can also infer magnetic field strengths where 1665 and 1667 MHz masers overlap, since the transitions undergo different Zeeman splitting for a given magnetic field strength. These values are presented in parentheses in Figure 1 and listed in Table 3. Near VLA 2 we find magnetic fields of 26.6 and 40.4 mG (Fig. 2), consistent in sign and (at least in the latter case) magnitude with values obtained by Slysh & Migenes (2006). (We note that the random error in the magnetic field strength es-

Electronic address: vfish@nrao.edu
[1] Jansky Fellow, National Radio Astronomy Observatory, 1003 Lopezville Road, Socorro, NM 87801
[2] Harvard–Smithsonian Center for Astrophysics, 60 Garden St., MS 42, Cambridge, MA 02138

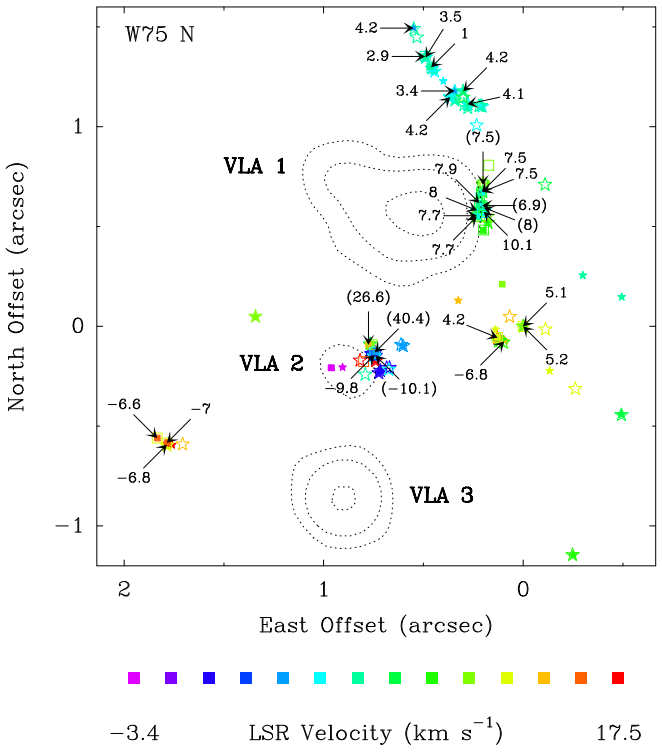

FIG. 1.— Map of detected OH maser emission in W75 N (epoch 2004 Sep 16/19). Stars indicate 1665 MHz emission, and squares indicate 1667 MHz emission. Open (filled) symbols denote emission in RCP (LCP). The LSR velocity of the peak of each maser profile is indicated in color. Numbers indicate magnetic fields derived from Zeeman splitting, with positive values representing fields oriented in the hemisphere away from the observer. Values in parentheses are deduced from overlaps in different transitions (see Tab. 3). X-band (8.4 GHz) continuum emission is shown in dotted contours. The feature at the origin is the same as the reference feature of Slysh & Migenes (2006), who give its absolute position as $20^h38^m36^s.416, +42°37'34''.42(\pm 0''.01)$ (J2000, epoch 2001 Jan 01).

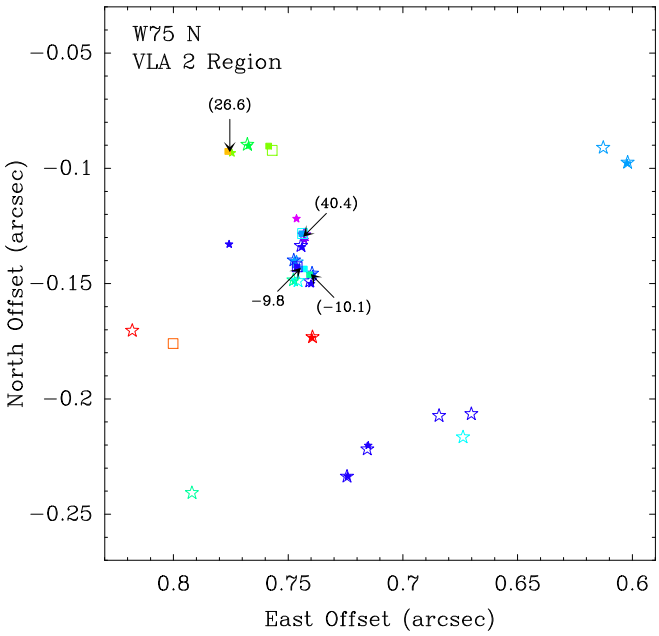

FIG. 2.— Enlargement of region near VLA 2. See Figure 1 for details. The continuum contours have been suppressed.

timate from multi-transition overlap may be somewhat larger than from traditional Zeeman pairs, since it is not known a priori that the 1665 and 1667 MHz Zeeman patterns are centered at the same systemic velocity. Nevertheless, this technique generally results in magnetic field estimates consistent with values obtained from proper Zeeman pairs, as can be seen near VLA 1 as well as in other sources (Fish & Reid, in preparation).)

Reanalyzing the data from epoch 1, we agree with Slysh & Migenes (2006) that spots 109 and 110 in Table 15 of Fish et al. (2005) form a 42.5 mG Zeeman pair at 1667 MHz (with multi-transition confirmation from spot 67 at 1665 MHz). Spots 112 and 113 also form a 34.5 mG Zeeman pair (approximately consistent with v_{LSR} of nearby 1665 MHz LCP spots 69 and 70). However, not all overlaps are indicative of magnetic fields. It is unlikely that spots 68 and 107 arise from a 137 mG magnetic field, as this would imply a systemic velocity v_{LSR} = 40.5 km s^{-1}, well above the maximum of detected masers in the region (Yngvesson et al. 1975).

The spectrum of recovered maser emission is shown in Figure 3. In each velocity channel, the total flux density of each (elliptical Gaussian) fitted maser spot is summed. The strongest maser we detect is located at $(\Delta\alpha, \Delta\delta)$ = (739.60, −145.53) and is approximately 400 Jy in both RCP and LCP ($2kT/A$). The equal flux densities suggest that the maser may be nearly 100% linearly polarized, as noted by Alakoz et al. (2005). Other masers near VLA 2 also show very high linear polarization fractions (Baart et al. 1986; Slysh et al. 2001; Hutawarakorn et al. 2002; Fish et al. 2005). The strongest spot is over twice as strong as in epoch 1 (Fish et al. 2005) and is stronger than measured on 2004 October 20 by Alakoz et al. (2005). It is unclear whether the same maser spot is experiencing a second flare or a different, nearby maser spot is undergoing a flare episode.

Proper motions of the OH masers are shown in Figure 4. Since the data for both epochs were phase referenced to a maser spot rather than an external source, our data cannot distinguish between the map presented and any other frame with a single constant vector added to all motions. In Figure 4 we have chosen the frame that minimizes the total length of all arrows not associated with VLA 2. The average speed of all masers excluding those near VLA 2 is 3.4 ± 2.1 km s^{-1}. This speed is comparable to that of OH masers around other young ultracompact H II regions, such as W3(OH) and ON 1 (Bloemhof et al. 1992, Fish & Reid, in preparation). The random error on the motion of an individual maser spot, given by the uncertainties in determining the position centroid in each epoch, ranges from negligible to 1.4 km s^{-1} with a median value of 0.2 km s^{-1}.

The presence of a disk associated with VLA 1 has often been inferred from the north-south distribution of OH masers (e.g., Haschick et al. 1981; Slysh et al. 2001). Indeed, the distribution of LSR velocity increases from north to south along this structure (e.g., Fig. 1). However, the proper motions of the OH masers are less clear. Figure 4 shows the average proper motions of clusters of masers along and south of the putative disk, relative to the cluster nearest the continuum emission (velocity "0"). Positive values indicate net motion away from this cluster. Proper motions in the south show clear organization away from the "0" cluster, but the motions of the northernmost clusters are mixed. Alternatively, the masers may be tracing a shocked, expanding layer (Baart et al. 1986). If so, the maser motions in the northernmost cluster may include a streaming component along an organized magnetic field (Fish & Reid 2006), with the caveat that while the field direction appears to be oriented along the distribution of masers, the external Faraday rotation contribu-

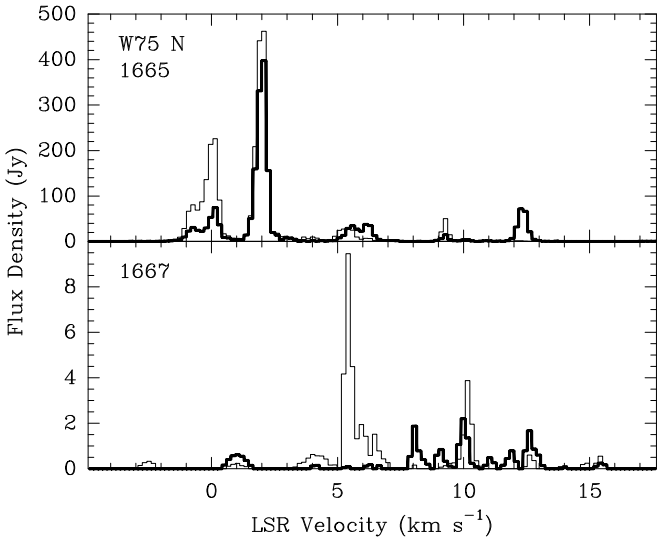

FIG. 3.— Spectrum of recovered maser emission in W75 N on 2004 September 16/19. RCP emission is shown in bold and LCP emission in normal weight.

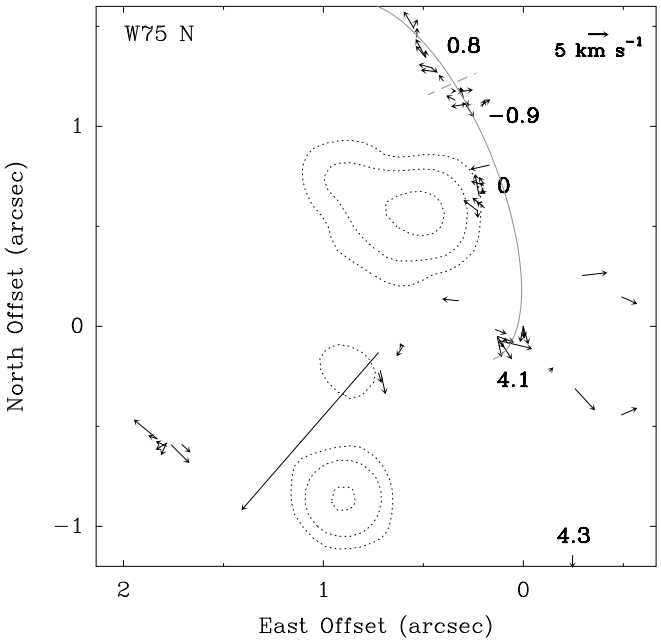

FIG. 4.— Proper motions of OH masers. Arrow lengths arge proportional to velocity as indicated in the upper right, assuming a distance of 2.0 kpc. The very long arrow corresponds to the motion of the 400 Jy maser near VLA 2. The reference frame has been chosen to minimize the total motion of masers not associated with VLA 2. Numbers indicate proper motions in km s^{-1} with respect to the cluster labelled "0" (positive indicates expansion). The gray curve shows the approximate location of the disk from Slysh et al. (2001).

tion is unknown (see also Slysh et al. 2002).

The motion of the 400 Jy maser (feature 70 in Table 1) near VLA 2 is over 50 km s^{-1}. Other than this particular maser, it is difficult to conclusively identify masers from one epoch to the next near VLA 2 due to variability and the large number of masers in the region. The distribution of masers near VLA 2 is also changing rapidly, as can be seen from comparison of Figure 2 with Figure 28 of Fish et al. (2005). LSR velocity is not necessarily a reliable indicator, as the masers appear to be accelerating. The brightest maser in the region has seen a change in velocity Δv_{LSR} = –0.45 km s^{-1} between the two epochs. Alakoz et al. (2005) note a similar decrease in v_{LSR} of this feature over a 2.5-year timescale.

The easternmost cluster of OH masers may be associated with another exciting source not seen in the continuum maps. The velocity of this cluster corrected for Zeeman splitting is $\sim$ 14 km s^{-1}, higher than any other cluster in W75 N (except for portions of VLA 2, which has a huge velocity scatter and no clear organization). Additionally, the maser proper motions are suggestive of slow ($\sim$ 5 km s^{-1}) expansion from a point in the center of the cluster (Fig. 4). This motion is likely preferentially in the plane of the sky in light of the small LSR velocity scatter of the masers.

4. DISCUSSION

It is difficult to track OH motions from the first epoch to the second epoch near VLA 2, both due to variability and the fast motions involved. These properties may be interrelated. It is probably not a coincidence that the two strongest ($>$ 100 Jy) masers in W75 N (features 70 and 73) both appear in the complicated cluster around VLA 2. While a connection between kinetic energy and H_2O maser flux density has been clearly established (Anglada et al. 1996), such a correlation is far less clear for OH, which is believed to be predominantly radiatively pumped. Nevertheless, regions with energetic motions may change the balance of pumping routes in favor of those with collisional components, possibly increasing the net pump rates in certain ground-state lines. (For a fuller discussion in a different context, see Gray et al. (2005).) We speculate that the energy source powering the VLA 2 outflow also helps to produce one of the strongest OH masers in the sky.

In most OH maser sources, it is fairly well established that the observed proper motions of the masers correspond to motions of physical clumps of material (see Bloemhof et al. 1996 and Fish & Reid, in preparation). But it is perhaps possible that the apparent motion of the brightest maser in VLA 2 is due to the passage of a fast-moving shock front through different portions of a cloud of OH rather than the ballistic motion of a single high-velocity clump of material. In any event, it appears that most individual maser spots near VLA 2 do not persist over timescales of years or longer. Multi-epoch phase-referenced VLBI observations spaced several months apart will be essential to track the motions of the OH masers around VLA 2. Phase referencing to a nearby bright calibrator would eliminate the ambiguity of the absolute position of the reference spot in each epoch. Despite this ambiguity in our data, it is clear that the 50 km s^{-1} motion of feature 70 in Table 1 with respect to the other masers in W75 N is due to a large intrinsic motion of feature 70 itself, since the velocity scatter (both from proper motions and radial velocities) of the rest of the W75 N masers is small.

Argon et al. (2003) report on a class of OH masers associated with outflows. For an OH maser in the Turner-Welch (TW) object near W3(OH), they obtain a (projected) proper motion of 66 km s^{-1} with Δv_{LSR} = 0.5 km s^{-1} over a period of 8 years. This is remarkably similar to what is seen near VLA 2. A key difference, however, is that the water masers in the TW object span a range in v_{LSR} of about 100 km s^{-1} (Cohen 1979; Hachisuka et al., in preparation) with proper motions of several tens of km s^{-1}. In comparison, the water masers in VLA 2 span a range of about 25 km s^{-1}, are arranged in a fairly organized circular pattern, and appear to be expanding at $\sim$ 28 km s^{-1} (Torrelles et al. 2003), slower than the OH masers.

The magnetic field near VLA 2 appears to undergo a line-of-sight reversal across this very compact source. (We note

the caveat, however, that three of the four magnetic field measurements are inferred from multi-transition overlap rather than single-transition Zeeman splitting.) Given the rapidly changing nature of this source, it would be fruitful to attempt confirmation of the magnetic field at another epoch, especially since new masers that appear may provide magnetic field information in regions presently unprobed by Zeeman splitting. The polarity of the field may be important if, for instance, the masers trace a magnetically-collimated outflow (Cunningham et al. 2005). While the exact relation between magnetic field strength (B) and density (ρ) may depend on the particular model (e.g., Pudritz et al. 2006), it is possible that 40 mG magnetic fields do not necessarily imply the extremely large densities that would be obtained from collapse models, where $B \propto \rho^{\kappa}, \kappa \approx 0.5$ (Crutcher 1999). Possibly these masers are from material being ejected from a protostellar disk, which may involve strong magnetic fields originating in the disk. Future observations may also be able to determine whether the unusually strong magnetic field at the OH masers in VLA 2 is decaying as in Cep A (Cohen et al. 1990; Bartkiewicz et al. 2005).

The National Radio Astronomy Observatory is a facility of the National Science Foundation operated under cooperative agreement by Associated Universities, Inc.

Facility: VLBA

REFERENCES

Alakoz, A. V., Slysh, V. I., Popov, M. V., & Val'tts, I. E. 2005, Astronomy Letters, 31, 375
Anglada, G., Estalella, R., Pastor, J., Rodríguez, L. F., & Haschick, A. D. 1996, ApJ, 463, 205
Argon, A. L., Reid, M. J., & Menten, K. M. 2003, ApJ, 593, 925
Baart, E. E., Cohen, R. J., Davies, R. D., Norris, R. P., & Rowland, P. R. 1986, MNRAS, 219, 145
Bartkiewicz, A., Szymczak, M., Cohen, R. J., & Richards, A. M. S. 2005, MNRAS, 361, 623
Bloemhof, E. E., Moran, J. M., & Reid, M. J. 1996, ApJ, 467, L117
Bloemhof, E. E., Reid, M. J., & Moran, J. M. 1992, ApJ, 397, 500
Cohen, N. L. 1979, Astrophys. Lett., 20, 81
Cohen, R. J., Brebner, G. C., & Potter, M. M. 1990, MNRAS, 246, 3P
Crutcher, R. M. 1999, ApJ, 520, 706
Cunningham, A., Frank, A., & Hartmann, L. 2005, ApJ, 631, 1010
Fish, V. L., & Reid, M. J. 2006, ApJS, 164, 99
Fish, V. L., Reid, M. J., Argon, A. L., & Zheng, X.-W. 2005, ApJS, 160, 220
Goedhart, S., Gaylard, M. J., & van der Walt, D. J. 2004, MNRAS, 355, 553
Gray, M. D., Howe, D. A., & Lewis, B. M. 2005, MNRAS, 364, 783
Harvey, P. J., Booth, R. S., Davies, R. D., Whittet, D. C. B., & McLaughlin, W. 1974, MNRAS, 169, 545
Haschick, A. D., Reid, M. J., Burke, B. F., Moran, J. M., & Miller, G. 1981, ApJ, 244, 76
Hunter, T. R., Taylor, G. B., Felli, M., & Tofani, G. 1994, A&A, 284, 215
Hutawarakorn, B., Cohen, R. J., Brebner, G. C. 2002, MNRAS, 330, 349
Lekht, E. E., & Krasnov, V. V. 2000, Astronomy Letters, 26, 38
Persi, P., Tapia, M., & Smith, H. A. 2006, A&A, 445, 971
Pudritz, R. E., Rogers, C. S., & Ouyed, R. 2006, MNRAS, 365, 1131
Shepherd, D. S., Testi, L., & Stark, D. P. 2003, ApJ, 584, 882
Shepherd, D. S., Kurtz, S. E., & Testi, L. 2004, ApJ, 601, 952
Slysh, V. I., & Migenes, V. 2006, MNRAS, 369, 1497
Slysh, V. I., Migenes, V., Val'tts, I. E., Lyubchenko, S. Yu., Horiuchi,, S., Altunin, V. I., Fomalont, E. B., & Inoue, M. 2002, ApJ, 564, 317
Slysh, V. I., Val'tts, I. E., & Migenes, V. 2001, Astronomy Reports, 45, 942
Torrelles, J. M., Gómez, J. F., Rodríguez, L. F., Ho, P. T. P., Curiel, S., & Vázquez, R. 1997, ApJ, 489, 744
Torrelles, J. M., et al. 2003, ApJ, 598, L115
Uscanga, L., Cantó, J., Curiel, S., Anglada, G., Torrelles, J. M., Patel, N. A., Gómez, J. F., & Raga, A. C. 2005, ApJ, 634, 468
Yngvesson, K. S., Cardiasmenos, A. G., Shanley, J. F., Rydbeck, O. E. H., & Elldér, J. 1975, ApJ, 195, 91

TABLE 1
DETECTED MASER SPOTS

Freq. (MHz)	Maser Feature	Δ RA (mas)	Δ Dec (mas)	v_{LSR} (km s^{-1})	Brightness (Jy beam^{-1})	Polarization
1665	1	–493.39	147.93	6.83	0.35	L
	2	–491.55	–440.64	7.35	0.07	L
		–491.89	–443.17	7.35	0.06	R
	3	–298.29	256.13	5.95	1.03	L
	4	–260.68	–312.38	12.74	1.22	R
	5	–246.81	–1144.76	9.84	0.25	R
		–249.22	–1145.51	9.81	0.13	L
	6	–132.16	–221.87	12.10	0.06	L
	7	–111.20	–14.49	12.80	0.82	R
	8	–109.22	710.59	8.23	0.15	R
	9	–0.24	–0.17	9.27	38.71	L
		0.16	0.37	9.28	2.89	R
	10	0.00	0.00	12.36	72.01	R
	11	68.21	49.04	13.17	0.24	R
	12	91.69	–70.85	13.68	0.33	L
	13	99.89	–80.27	9.64	0.15	R
	14	115.69	–71.09	9.45	0.41	R
	15	124.48	–74.32	10.01	0.25	R
	16	127.59	–55.61	12.09	0.25	L
	17	129.00	–58.36	14.56	0.06	R
	18	129.22	–48.70	13.33	0.23	L
	19	138.83	–14.49	12.80	1.25	L
	20	177.24	520.20	9.99	0.58	R
		177.24	520.20	9.99	0.27	L
	21	178.97	550.75	10.16	0.23	R
	22	193.50	579.87	9.99	0.13	R
	23	193.54	581.00	5.24	0.14	R
	24	196.35	595.53	8.97	1.13	R
	25	200.58	718.00	11.22	0.34	R
	26	200.94	707.45	10.87	1.11	R
	27	201.09	568.85	4.01	1.17	L
	28	203.33	673.95	4.54	0.19	L

TABLE 1 — *Continued*

Freq. (MHz)	Maser Feature	Δ RA (mas)	Δ Dec (mas)	v_{LSR} (km s^{-1})	Brightness (Jy beam^{-1})	Polarization
	29	203.33	673.95	8.96	0.68	R
	30	205.54	605.61	9.26	11.32	R
	31	206.33	1102.14	5.49	6.55	R
		205.82	1102.49	5.42	0.91	L
	32	211.63	1106.88	5.90	3.03	R
	33	212.98	613.36	4.56	1.37	L
	34	221.71	1104.56	5.95	0.39	R
	35	230.48	581.26	5.41	4.10	L
		230.63	581.31	5.48	0.44	R
	36	231.83	581.66	10.15	0.43	R
	37	231.93	549.56	10.11	3.08	R
	38	233.01	558.86	5.55	11.66	L
		233.29	559.16	5.53	2.43	R
	39	233.47	1007.83	5.24	0.26	R
	40	277.46	1114.03	6.50	0.45	R
	41	277.89	1094.50	5.82	6.05	R
		279.11	1097.13	5.59	0.92	L
	42	282.51	1113.27	4.07	5.63	L
		278.85	1113.22	4.22	0.28	R
	43	297.23	1111.03	6.85	0.90	R
	44	300.27	1178.27	3.21	0.84	L
	45	300.94	1147.54	7.35	0.25	R
	46	301.64	1178.27	5.70	4.93	R
		301.59	1178.09	5.59	3.25	L
	47	325.79	130.03	13.90	0.41	L
	48	342.64	1177.95	5.51	15.39	R
		342.01	1178.43	5.57	1.66	L
	49	343.12	1133.25	6.52	2.57	R
		342.91	1132.95	6.47	0.39	L
	50	346.17	1180.21	3.48	0.38	L
	51	365.98	1147.96	4.54	0.26	L
		365.89	1148.01	4.54	0.08	R
	52	367.61	1149.59	7.01	0.18	R
	53	400.92	1229.55	4.71	0.56	L
	54	445.02	1276.97	5.31	1.00	L
		444.40	1277.38	5.15	0.32	R
	55	457.52	1293.28	5.15	7.49	L
		457.14	1292.72	5.18	4.64	R
	56	488.92	1347.51	5.16	6.15	L
		488.92	1347.51	5.07	0.18	R
	57	489.71	1348.16	7.21	0.74	R
	58	490.24	1347.86	5.18	1.05	R
	59	533.26	1448.99	7.00	0.16	R
	60	548.23	1491.99	6.15	0.48	R
	61	550.47	1496.78	3.69	5.04	L
	62	602.08	–97.43	3.11	2.03	R
		602.28	–97.74	3.14	1.30	L
	63	612.70	–91.00	3.13	0.85	R
	64	670.20	–206.46	0.50	0.51	R
	65	673.82	–216.53	4.54	0.23	R
	66	684.26	–207.25	0.67	0.47	R
	67	715.54	–221.75	0.67	0.43	R
		715.14	–220.16	0.85	0.36	L
	68	724.38	–233.62	0.60	0.34	R
		724.16	–233.53	0.67	0.32	L
	69	739.42	–173.13	17.40	0.13	R
		739.72	–173.37	17.39	0.08	L
	70	739.60	–145.53	2.00	408.83	R
		739.39	–145.95	1.98	402.02	L
	71	740.07	–150.02	–0.12	51.31	L
		740.61	–148.88	–0.13	9.32	R
	72	742.92	–130.89	–0.77	52.19	L
		743.08	–128.94	–0.75	23.14	R
	73	744.08	–134.10	0.09	134.88	L
		744.44	–133.57	0.11	59.95	R
	74	745.71	–148.79	4.26	0.48	R
	75	746.35	–140.72	3.09	1.25	R
	76	746.38	–121.79	–3.37	0.73	L
	77	747.32	–140.04	2.69	5.61	L
		747.57	–139.85	2.43	4.58	R
	78	747.74	–148.44	6.21	34.73	R
		747.34	–148.90	6.23	4.89	L
	79	767.28	–90.12	7.14	1.08	L
		767.82	–89.66	7.23	0.32	R
	80	774.58	–93.27	10.87	0.14	L
	81	775.76	–132.90	0.85	0.39	L

TABLE 1 — *Continued*

Freq. (MHz)	Maser Feature	Δ RA (mas)	Δ Dec (mas)	v_{LSR} (km s^{-1})	Brightness (Jy beam^{-1})	Polarization
	82	791.97	–240.71	5.83	1.72	R
	83	817.99	–170.32	17.24	0.57	R
	84	905.22	–204.56	–2.32	0.30	L
	85	1341.64	49.55	11.39	0.14	R
		1341.26	48.92	11.39	0.11	L
	86	1706.84	–590.03	13.68	0.35	R
	87	1759.06	–592.88	16.49	0.07	L
	88	1784.06	–587.59	16.14	0.07	L
	89	1785.98	–596.61	12.16	6.42	R
		1785.19	–596.61	12.14	0.30	L
1667	90	1.10	–0.61	11.89	0.76	R
	91	1.39	–0.06	10.09	0.39	L
	92	105.78	211.80	10.19	1.09	L
	93	129.66	–54.79	12.62	0.49	R
		129.75	–54.81	12.67	0.45	L
	94	173.09	807.56	11.06	0.22	R
	95	195.97	575.29	6.47	0.15	L
	96	197.78	595.08	8.02	0.66	R
	97	198.82	482.75	9.11	0.54	R
		199.99	480.96	9.11	0.06	L
	98	202.42	708.63	9.98	1.69	R
	99	203.25	568.73	5.42	0.31	L
		203.40	570.11	5.42	0.10	R
	100	206.94	605.17	8.45	0.42	R
	101	207.18	674.50	5.42	5.08	L
	102	207.81	673.79	8.09	0.94	R
	103	219.18	618.12	8.05	0.10	R
	104	219.78	617.31	5.24	0.27	L
	105	222.44	655.77	6.01	1.30	L
	106	233.08	549.21	9.20	0.32	R
	107	233.66	550.95	6.49	0.61	L
	108	457.98	1295.24	6.30	0.14	R
	109	465.01	1301.25	5.95	0.07	L
	110	491.50	1353.89	6.64	0.13	R
	111	491.93	1351.43	5.62	0.47	L
	112	740.70	–146.15	6.79	0.35	L
	113	742.94	–143.59	4.48	0.37	L
	114	744.02	–128.38	4.00	0.47	L
		743.76	–128.26	4.07	0.13	R
	115	746.10	–142.66	1.02	0.61	R
		746.14	–142.78	1.00	0.18	L
	116	758.52	–90.35	10.17	0.55	L
		756.98	–92.17	10.07	0.36	R
	117	776.37	–92.64	14.01	0.11	L
	118	800.17	–175.96	15.46	0.25	R
	119	962.06	–207.57	–2.53	0.14	L
	120	1784.15	–582.29	15.41	0.21	L
	121	1786.02	–584.16	12.94	0.25	R
	122	1833.33	–559.66	14.90	0.12	L
	123	1833.95	–559.60	12.56	0.79	R

NOTE. — Coordinates are position offsets from the reference feature located at the origin. Spots detected at the same location in RCP and LCP at nearly the same LSR velocity are treated as a single feature, as in Fish et al. (2005).

TABLE 2
ZEEMAN PAIRS

Frequency (MHz)	RCP Δ RA (mas)	RCP Δ Dec (mas)	RCP v_{LSR} (km s^{-1})	LCP Δ RA (mas)	LCP Δ Dec (mas)	LCP v_{LSR} (km s^{-1})	*B* (mG)	Separation (mas)	Pair Number[a]
1665	0.00	0.00	12.36	–0.24	–0.17	9.27	5.2	0.3	Z1
	99.89	–80.27	9.64	91.69	–70.85	13.68	–6.8	12.5	
	129.00	–58.36	14.56	127.59	–55.61	12.09	4.2	3.1	
	193.50	579.87	9.99	201.09	568.85	4.01	10.1	13.4	
	203.33	673.95	8.96	203.33	673.95	4.54	7.5	0.0	
	231.83	581.66	10.15	230.48	581.26	5.41	8.0	1.4	
	231.93	549.56	10.11	233.01	558.86	5.55	7.7	9.4	
	277.46	1114.03	6.50	282.51	1113.27	4.07[b]	4.1	5.1	
	301.64	1178.27	5.70	300.27	1178.27	3.21	4.2	1.4	
	342.64	1177.95	5.51	346.17	1180.21	3.48	3.4	4.2	
	367.61	1149.59	7.01	365.98	1147.96	4.54	4.2	2.3	
	489.71	1348.16	7.21	488.92	1347.51	5.16	3.5	1.0	Z3
	548.23	1491.99	6.15	550.47	1496.78	3.69	4.2	5.3	
	1785.98	–596.61	12.16	1784.06	–587.59	16.14	–6.8	9.2	

TABLE 2 — *Continued*

Frequency (MHz)	RCP Δ RA (mas)	RCP Δ Dec (mas)	RCP v_{LSR} (km s^{-1})	LCP Δ RA (mas)	LCP Δ Dec (mas)	LCP v_{LSR} (km s^{-1})	*B* (mG)	Separation (mas)	Pair Number[a]
1667	1.10	–0.61	11.89	1.39	–0.06	10.09	5.1	0.6	
	207.81	673.79	8.09	207.18	674.50	5.42	7.5	1.0	Z2
	219.18	618.12	8.05	219.78	617.31	5.24	7.9	1.0	
	233.08	549.21	9.20	233.66	550.95	6.49	7.7	1.8	
	457.98	1295.24	6.30	465.01	1301.25	5.95	1.0	9.3	
	491.50	1353.89	6.64	491.93	1351.43	5.62	2.9	2.5	
	746.10	–142.66	1.02	742.94	–143.59	4.48	–9.8	3.3	
	1786.02	–584.16	12.94	1784.15	–582.29	15.41	–7.0	2.6	
	1833.95	–559.60	12.56	1833.33	–559.66	14.90	–6.6	0.6	

[a] Pair number listed in Table 1 of Slysh & Migenes (2006).[b] Alternatively, this may form part of a loose complete 5.6 mG Zeeman pattern with spot 45 and another linearly-polarized spot. See Fish & Reid (2006).

TABLE 3
MAGNETIC FIELDS INFERRED FROM MULTI-TRANSITION OVERLAP

Frequency (MHz)	Pol.	Δ RA (mas)	Δ Dec (mas)	v_{LSR} (km s^{-1})	Frequency (MHz)	Pol.	Δ RA (mas)	Δ Dec (mas)	v_{LSR} (km s^{-1})	*B* (mG)	Separation (mas)
1665	R	196.35	595.53	8.97	1667	R	197.78	595.08	8.02	8.0	1.5
1665	R	200.94	707.45	10.87	1667	R	202.42	708.63	9.98	7.5	1.5
1665	R	205.54	605.61	9.26	1667	R	206.94	605.17	8.45	6.9	1.5
1665	R	739.60	–145.53	2.00	1667	L	740.70	–146.15	6.79	–10.1	1.3
1665	L	742.92	–130.89	–0.77	1667	L	744.02	–128.38	4.00	40.4	2.7
1665	L	774.58	–93.27	10.87	1667	L	776.37	–92.64	14.01	26.6	1.9